Computer-Aided Design 115 (2019) 52–63

Contents lists available at ScienceDirect

Computer-Aided Design

journal homepage: www.elsevier.com/locate/cad

Free isotropic material optimization via second order cone programming☆,☆☆

Xingtong Yang, Ming Li *

State Key Laboratory of CAD&CG, Zhejiang University, Hangzhou, China

ARTICLE INFO

Article history:
Received 24 April 2019
Accepted 3 May 2019

Keywords:
Free isotropic material optimization (FIMO)
Second order cone programming
Poisson's ratio
Multi-material
Topology optimization

ABSTRACT

Designing an engineered structure of optimal performance is the ultimate goal of engineering design, and various structural optimization approaches have been proposed. However, previous studies on the topic mainly rely on the single design variable of Young's modulus or density without considering its Poisson's ratio as another key isotropic material parameter, and thus may limit the best design ultimately reached. In the study, the problem of *free isotropic material optimization (FIMO)* is studied that takes as design variables both Young's modulus and Poisson's ratio at each point of the design domain without constraints on its manufacturability; certain necessary conditions on the material attainability are the only imposed requirements. Global optimum to the FIMO is achieved via rigorously reformulating it as a second order cone programming, to which a global optimum is theoretically verified and numerically trackable; the novel formulation also avoids the challenging singularity issue on void elements. The material dimension of the resulted design can also be reduced to any prescribed number of high fidelity via a hierarchical material clustering algorithm. The generated structure can be taken as benchmark solutions with which other optimized designs can be compared, and to propose novel new product design. Performance of the approach is tested on various 2D examples, in comparison with structures generated via classical topology optimization.

1. Introduction

Designing a structure of desirable optimal performance is the ultimate goal of engineering and product design. It can be achieved via structural optimization methods that find the optimal geometric parameters or shapes or even topologies driven by their associated physical properties, which approach is respectively called parametric optimization, shape optimization or topology optimization [1]. In particular, topology optimization aims to find the best solid-void distribution within a discrete design domain for improved structural performance. The approaches have undergone tremendous development in the last decades [1–5], and have produced various novel optimized structures of extreme properties [6] and found wide industrial applications [7,8].

In traditional studies on topology optimization [2–4,9,10], mainly Young's modulus associated to each design element is directly or implicitly taken as the design variable, ignoring other important material parameters such as Poisson's ratio or general anisotropy. It thus may limit the performance that the optimized structure can ultimately reach. Indeed, multi-scale topology optimization approaches have also been proposed that compute an optimized microstructure to each macro-element [11–15], which possesses a target homogenized material tensor so that the macro-property of the final design can be further improved. The approaches manifest the ultimate design target that the designers aim to achieve, but in practice may encounter difficulties in convergence control, tremendous computational efforts, unconnected microstructures, or discontinuity between adjacent microstructures, owning to its complexity in geometric control and property analysis. Researchers have thus also devoted efforts to separating the process as two consequent steps of first optimizing material distribution within the macro-structure, which is then to guide the microstructure design associated with each macro-element. However, as the macro-structure is generally optimized solely based on its Young's modulus [4,16,17], performance of the optimized design is generally not improved from

☆ This paper has been recommended for acceptance by Pierre Alliez, Yong-Jin Liu & Xin Li.

☆☆ No author associated with this paper has disclosed any potential or pertinent conflicts which may be perceived to have impending conflict with this work. For full disclosure statements refer to https://doi.org/10.1016/j.cad.2019.05.002.

* Corresponding author.
E-mail address: liming@cad.zju.edu.cn (M. Li).

https://doi.org/10.1016/j.cad.2019.05.002
0010-4485/

this embedding process, and the potentiality of the multiscale optimization is not fully utilized.

In order to resolve this issue and to step further to designing the "best" structure of extreme physical performance, a free isotropic material optimization (FIMO) problem is studied here. The material isotropy means that its elastic property (or specifically its material tensor) is uniform in all orientations, represented using its Young's modulus and Poisson's ratio, which are both taken as design variables in FIMO. The material is free in the sense that the material tensor can vary at each point of the design domain without constraints on its manufacturability; the only imposed requirements on the material tensor are certain necessary conditions on its attainability. The material distribution is optimized to meet the design target. The generated structure can be considered as the best structure among possible elastic continua [18,19], and used as benchmark solutions with which other structural designs can be compared and to stimulate novel designs. In addition, the derived structure can also be used in generating an optimal isotropic porous structure via embedding associated microstructures, which is to be explored in our future work.

Poisson's ratio has an impressive effect in designing high-stiffness composites, and has attracted research efforts on its usage for further structural performance improvement. For instance, Liu et al. found that the effective Young's modulus of laminated two-phase composites would exceed the Voigt estimation or that of each individual constituent phase [20] when one of the constituent phases is close to the thermodynamic limit. Significant stiffness enhancement was also found when incorporating negative Poisson's ratio (NPR) inclusions into composites in [21]. Successive study was also conducted to investigate the influence of Poisson's ratio of constituent, or topologies of NPR inclusions, in composites [22,23]. Recently, Long et al. found from numerical results that the Poisson effect plays a key role in reducing the mean compliance of the final design in multi-material composite structures [24], and considering negative Poisson's ratio results in lower compliance than the single-scale optimization.

One main challenge of the FIMO problem comes from the ultimate goal to numerically compute the global optima to the originally nonlinear and non-convex optimization problem. We show here that the use of the complementary energy can reformulate the problem as a second order cone programming (SOCP) which has a theoretically proved global optimality. SOCP is a special and important class of nonlinear numerical optimization problems widely studied, and has special conic optimizer MOSEK [25] and has been implemented in commercial optimization software CPLEX [26]. It has also been studied in design optimization for frame and trusses [27–32] but no solution for general FE analysis was found before. Note that the FMO (Free Material Optimization) problem [18,19,33–37], where all the material elasticity tensor components are taken as design variables, is usually formulated as a nonlinear semidefinite programming (SDP) which is a hyperset of SOCP and is usually more challenging to devise efficient numerical approaches. Compared to classic topology optimization approaches [4,38], the FMO problem formulated via SDP or the novel FIMO formulated via SOCP, has another advantage that it does not involve any FEA computations during optimization, by avoiding solving the original mechanical equilibrium equations. It is thus easy to be implemented and, in particular, naturally avoids the challenging singularity issue caused by void elements involved in the FE analysis of the design.

An inherent difficulty associated to the FIMO problem is the attainability or manufacturability of the optimized material elasticity tensors. It in fact has been proved that any positive definite fourth order tensor, which satisfies the symmetries of an elasticity tensor, is always attainable using a stiff enough material [39]. However, it still remains open to prescribe well-founded mathematical constraints so that the microstructure can be attained for given candidate materials [37,40]. In practice, people tend to utilize lower and upper bounds on the trace of the elasticity tensor as constraints on the material resource, which is also applied in this study. In addition, a material clustering approach is also proposed in this study to reduce the material variety, which is also able to help to ultimately produce a manufacturable structure with optimized performance and to reduce computational costs of downstream tasks.

In summary, the novelty and contributions of the study include three main aspects. Firstly, the novel FIMO problem is introduced and studied that includes Poisson's ratio as design variables to find the best isotropic structure. Secondly, the problem is rigorously reformulated as SOCP which has theoretically proved global optima and well developed numerical approaches. The novel SOCP formulation does not involve any FEA computation, and avoids the challenging singularity issue caused by void elements. Thirdly, a hierarchical material clustering algorithm is developed to reduce the design space to any prescribed number of a high structural fidelity. The approach is tested on various 2D examples and demonstrates high effectivity in comparison with classical benchmark results.

The remainder of the paper is arranged as follows. The FIMO problem is formulated in Section 2. Approaches to converting it to an SOCP problem are detailed in Sections 3 and 4, and the material clustering approach is explained in Section 5. After presenting various 2D examples in Section 6, the paper is concluded in Section 7.

2. Problem formulation

Given a linear elasticity analysis problem, the *free isotropic material optimization (FIMO)* aims to find the optimal distribution of a group of isotropic material tensors, in terms of their Young's modulus and Poisson's ratios, within a design domain under certain boundary conditions, for which the structure is as effective as possible. The widely studied problem of minimum compliance, or equivalently maximum stiffness, is examined here.

To get a computationally tractable model, a finite element approximation is used. Suppose $\Omega = \{\Omega_e,\ e = 1 \dots N\}$ is a discrete design domain consisting of N disjoint square FE elements Ω_e of the same size. The material is assumed to be constant within each cell. Let $E_e > 0, -1.0 < \nu_e < 0.5 \in \mathbb{R}$ be the associated Young's modulus and Poisson's ratio to each element $e = 1 \dots N$, and $\mathbf{D}_e(E_e, \nu_e)$ the 2D material elasticity tensor defined via,

$$\mathbf{D}_e(E_e, \nu_e) = \frac{E}{1-\nu^2}\begin{bmatrix} 1 & \nu & 0 \\ \nu & 1 & 0 \\ 0 & 0 & \dfrac{1-\nu}{2} \end{bmatrix}, \tag{1}$$

which is symmetric and positive semidefinite. We also define $\mathbf{E} = (E_1, \dots, E_N)$, $\boldsymbol{\nu} = (\nu_1, \dots, \nu_N)$ and $\mathbf{D} = (\mathbf{D}_1, \dots, \mathbf{D}_N)$ for simplicity. The trace of $\mathbf{D}_e(E_0, \nu_0)$ is calculated by

$$\mathrm{Tr}(\mathbf{D}_e(E_0, \nu_0)) = \frac{E_0(5-\nu_0)}{2(1-\nu_0^2)}. \tag{2}$$

Following the classical FE analysis, the displacement function in linear elasticity is approximated by a continuous function that is bilinear in each coordinate on every element, whose coefficients are represented by a discrete vector $\mathbf{u} \in \mathbb{R}^n$. The free isotropic material optimization (FIMO) problem is then stated as: find the optimal distribution of material tensors $\mathbf{D}$, or in terms of its Young's modulus $\mathbf{E}$ and Poisson's ratio $\boldsymbol{\nu}$, so that the

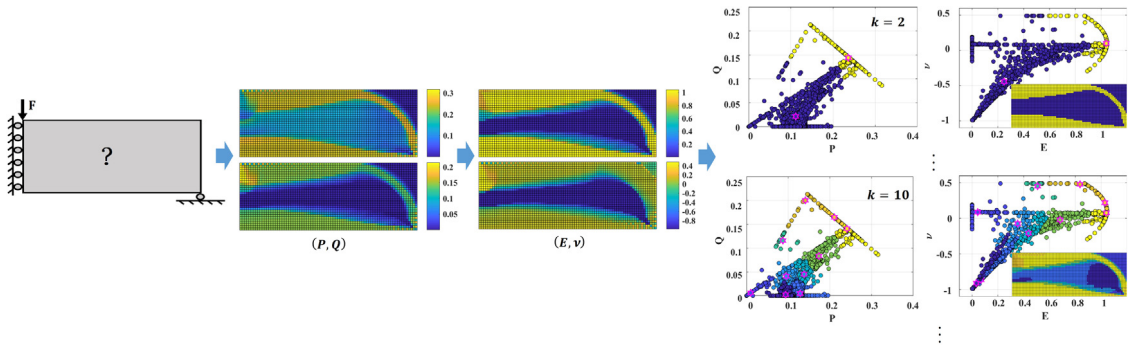

Fig. 1. Overview of the approach in solving free isotropic material optimization (FIMO) problem. The FIMO problem defined in (3) is first formulated as second order cone programming (SOCP) in a new (P, Q) space. The computed solution results in an globally optimal material distribution within the design domain. A multi-material domain of any prescribed material number is also able to be obtained using a carefully designed hierarchical clustering algorithm.

compliance of the resulted structure is minimized, that is,

$$\min_{\mathbf{E},\boldsymbol{\nu}\in\mathbb{R}^N} c(\mathbf{u},\mathbf{E},\boldsymbol{\nu}),\ s.t. \tag{3}$$

$$\begin{cases} \mathbf{K}(\mathbf{E},\boldsymbol{\nu})\mathbf{u}=\mathbf{f},\ \mathbf{u}\in\mathcal{U}, & \text{equilibrium equation}\\ \sum_{i=e}^{N}\mathrm{Tr}(\mathbf{D}_e)\le m_f T_0, & \text{global trace constraints}\\ \underline{T_e}\le\mathrm{Tr}(\mathbf{D}_e)\le\overline{T_e},\ 1\le e\le N, & \text{element trace constraints}\\ \nu_0<\nu_e\le\nu_1,\ 1\le e\le N, & \text{Poisson's ratio range}\end{cases}$$

where $\mathbf{f}$ is the exerted nodal force vector ignoring the structure weight for simplicity, and $\mathbf{u}$ and $\mathcal{U}\subset\mathbb{R}^d$ are the nodal displacement vector and its admissible space, where certain Dirichlet boundary conditions are prescribed.

In addition, $\underline{T_e}$ and $\overline{T_e}$ are the prescribed lower and upper bounds for the trace $\mathrm{Tr}(\mathbf{D}_e)$ of an element e. T_0 is the global trace for a reference structure fully filled with material of $E_0=1$, $\nu_0=0.3$ as widely adopted in structural optimization, and $m_f>0$ is a prescribed *material cost fraction*. These traces are used to described the 'cost' of the material [18,36]. ν_0 and ν_1 are the prescribed range of Poisson's ratio.

The global stiffness matrix $\mathbf{K}(\mathbf{E},\boldsymbol{\nu})$ of a finite element structure Ω with material distribution $\mathbf{D}(\mathbf{E},\boldsymbol{\nu})$ is calculated by

$$\mathbf{K}(\mathbf{E},\boldsymbol{\nu})=\sum_{e=1}^{N}\mathbf{K}_e(\mathbf{E},\boldsymbol{\nu}),\ \mathbf{K}_e(\mathbf{E},\boldsymbol{\nu})=\sum_{k=1}^{n_G}\mathbf{B}_{e,k}^T\mathbf{D}_e\mathbf{B}_{e,k}, \tag{4}$$

where $\mathbf{B}_{e,k}$ is the strain–displacement matrix and n_G is the number of Gaussian integration points, see e.g. [41]. Note that $\mathbf{K}$ and $\mathbf{K}_e$ are all symmetric positive semidefinite.

The objective function $c(\mathbf{u},\mathbf{E},\boldsymbol{\nu})$ is the structure's compliance and calculated by

$$c(\mathbf{u},\mathbf{E},\boldsymbol{\nu})=\frac{1}{2}\mathbf{u}^T\mathbf{K}(\mathbf{E},\boldsymbol{\nu})\mathbf{u}=\sum_{e=1}^{N}\frac{1}{2}\mathbf{u}_e^T\mathbf{K}_e(\mathbf{E},\boldsymbol{\nu})\mathbf{u}_e, \tag{5}$$

where $\mathbf{u}_e$ is the displacement vector associated to an element e.

In the proposed approach, as illustrated in Fig. 1, the FIMO problem is reformulated as SOCP via mapping the material space of (E,μ) to another space defined by new parameters (P,Q). Performing the optimization in (P,Q) space produces an optimal continua with free isotropic material tensor. In the end, the material space is greatly reduced if necessary via clustering the derived materials into a small number of different materials.

3. Fundamentals of compliance minimization of continua

The SOCP is first introduced in this section. Then the FIMO problem in Eq. (3) is reformulated into a form based on complementary energy, from which the SOCP formulation for the FIMO problem is derived in Section 4.

3.1. Second order cone programming

In a second-order cone programming (SOCP), a linear objective function is minimized over cone defined as the intersection of an affine set and the product of second-order (quadratic) cones. SOCPs are nonlinear convex problems which include linear and (convex) quadratic programs as special cases, but are less general than semidefinite programming (SDPs).

A second-order cone program (SOCP) is a convex optimization problem of the form: find $\mathbf{x}$ such that

$$\begin{aligned}\min_{\mathbf{x}}\quad & \mathbf{c}^T\mathbf{x}\\ s.t.\quad & \|\mathbf{A}_i\mathbf{x}+\mathbf{b}_i\|_2\le\mathbf{c}_i^T\mathbf{x}+d_i,\qquad i=1,\ldots,m\\ & \mathbf{F}\mathbf{x}=\mathbf{g},\end{aligned}$$

where $\mathbf{x}\in\mathbb{R}^n$ is the design variable, and the problem parameters are $\mathbf{c}\in\mathbb{R}^n$, $\mathbf{A}_i\in\mathbb{R}^{n_i\times n}$, $\mathbf{b}_i\in\mathbb{R}^{n_i}$, $\mathbf{c}_i\in\mathbb{R}^n$, $d_i\in\mathbb{R}$, $\mathbf{F}\in\mathbb{R}^{p\times n}$, $\mathbf{g}\in\mathbb{R}^p$.

Convex quadratically constrained quadratic programs can also be formulated as SOCPs by reformulating the objective function as a constraint. Semidefinite programming subsumes SOCPs as the SOCP constraints can be written as linear matrix inequalities and can be reformulated as an instance of semidefinite program using the Schur complement theorem. Further details on SOCP are referred to [27,29].

The following fact about second-order cone constraint is to be used later,

$$w^2\le xy,\ x\ge 0,\ y\ge 0\Leftrightarrow x+y\ge\left\|\begin{bmatrix}2w\\ x-y\end{bmatrix}\right\|. \tag{6}$$

3.2. Decomposed formulation based on complementary energy

The FIMO problem in (3) is first reformulated based on complementary energy in order to derive its SOCP formulation. A SOCP for truss and frame was previously derived in [28,31,32], constructed by Euler–Bernoulli beam elements. However, its extension to FE analysis is non-trivial, and is the first time derived in this study.

Given the vector of external force $\mathbf{f}\in\mathbb{R}^d$, the complementary energy theory tells the following fact: the compliance c of a structure defined in (5) can also be determined as follows:

$$c=2\sup\left\{\mathbf{f}^T\mathbf{u}-\frac{1}{2}\mathbf{u}^T\mathbf{K}\mathbf{u}\mid\mathbf{u}\in\mathbb{R}^d\right\}, \tag{7}$$

where sup refers to a function supremum.

Performing singular value decomposition for $\mathbf{K}_e$ gives its five non-zero eigenvalues $\{\lambda_{el}\}$ and the corresponding eigenvectors $\{\mathbf{b}_{el}\}$ in the following form:

$$\lambda = \left[\frac{E_e(3-\nu_e)}{6(1-\nu_e^2)} \quad \frac{E_e(3-\nu_e)}{6(1-\nu_e^2)} \quad \frac{E_e}{1+\nu_e} \quad \frac{E_e}{1+\nu_e} \quad \frac{E_e}{1-\nu_e}\right]^T \tag{8}$$

and

$$[\mathbf{b}_{e1}, \mathbf{b}_{e2}, \mathbf{b}_{e3}, \mathbf{b}_{e4}, \mathbf{b}_{e5}] = \begin{bmatrix} -1 & 0 & 0 & 1 & -1 \\ 0 & -1 & -1 & 0 & -1 \\ 1 & 0 & -1 & 0 & 1 \\ 0 & 1 & 0 & -1 & -1 \\ -1 & 0 & 0 & -1 & 1 \\ 0 & -1 & 1 & 0 & 1 \\ 1 & 0 & 1 & 0 & -1 \\ 0 & 1 & 0 & 1 & 1 \end{bmatrix}. \tag{9}$$

Note here that $\{\mathbf{b}_{el}\}$ are constant vectors. Accordingly, the stiffness matrix $\mathbf{K}_e$ can be rewritten as

$$\mathbf{K}_e = \sum_{l=1}^{5} k_{el}\mathbf{b}_{el}\mathbf{b}_{el}^T, \tag{10}$$

where

$$k_{e1} = k_{e2} = \frac{E_e(3-\nu_e)}{24(1-\nu_e^2)}, \quad k_{e3} = k_{e4} = \frac{E_e}{4(1+\nu_e)}, \quad k_{e5} = \frac{E_e}{8(1-\nu_e)}, \tag{11}$$

and the global stiffness matrix is straightforwardly built,

$$\mathbf{K} = \sum_{e=1}^{N}\sum_{l=1}^{5} k_{el}\mathbf{b}_{el}\mathbf{b}_{el}^T. \tag{12}$$

Note that in the decomposed form of Eq. (12) the material parameters (E, ν) only appear in the scalar items k_{el}, which is deliberately designed for the following transformation.

Substituting Eq. (12) into Eq. (7), we have

$$c = 2\sup\left\{\mathbf{f}^T\mathbf{u} - \sum_{e=1}^{N}\sum_{l=1}^{5}\frac{1}{2}k_{el}(\mathbf{b}_{el}^T\mathbf{u}_e)^2 \mid \mathbf{u} \in \mathbb{R}^d\right\}. \tag{13}$$

This is a convex quadratic optimization problem, which has the following dual problem,

$$c = \inf_{w_{el}, s_{el}}\left\{2\sum_{e=1}^{N}\sum_{l=1}^{5} w_{el} \mid w_{el}k_{el} \geq \frac{s_{el}^2}{2}, \ \forall e, l, \sum_{e=1}^{N}\sum_{l=1}^{5} s_{el}\mathbf{b}_{el} = \mathbf{f}\right\}. \tag{14}$$

In the above formulation, the equality constraint corresponds to the force-balance equation, and the inequality constraints are satisfied with equalities at an optimal solution. Meanwhile, $w_{e1}+w_{e2}+w_{e3}+w_{e4}+w_{e5}$ is equal to the complementary strain energy stored in member e. Note in Eq. (14) that each $\mathbf{b}_{el}$ is a constant vector. Thus, if taking the variables $k_{el} \in \mathbb{R}$ as independent variables, the problem in Eq. (14) can be directly formulated as an SOCP problem. Consequently, the FIMO problem in (3) becomes an SOCP. However, each $k_{el} \in \mathbb{R}$ in Eq. (14) is a nonlinear function in terms of the material Young's modulus and Poisson's ratio defined on each element member e, and formulating it as an SOCP is a challenging task. The issue is to be addressed next.

4. Free isotropic material optimization as SOCP

4.1. Young's modulus $\mathbf{E}$ as single design variable

We first study the simpler case that only Young's modulus $\mathbf{E}$ is taken as design variable, that is, given a fixed Poisson's ratio $\boldsymbol{\nu}$ and material constraints, optimize the distribution of Young's modulus of each element over the design domain to minimize the structural compliance.

In this case, the decomposition form of Eq. (10) is reduced to

$$\mathbf{K}_e = \sum_{l=1}^{5} E_e a_{el}\mathbf{b}_{el}\mathbf{b}_{el}^T \tag{15}$$

with

$$a_{e1} = a_{e2} = \frac{3-\nu_e}{24(1-\nu_e^2)}, \ a_{e3} = a_{e4} = \frac{1}{4(1+\nu_e)}, \ a_{e5} = \frac{1}{8(1-\nu_e)}. \tag{16}$$

Accordingly, the inequality constraints in Eq. (14) becomes

$$w_{el}E_e \geq \frac{s_{el}^2}{2a_{el}}, \ e = 1, \ldots, N, \quad l = 1, \ldots, 5. \tag{17}$$

From the facts of SOCP in Eq. (6), Eq. (17) is equivalently rewritten as a cone constraint,

$$w_{el} + E_e \geq \left\| \begin{bmatrix} w_{el} - E_e \\ \sqrt{2/a_{el}}s_{el} \end{bmatrix} \right\|, \ e = 1, \ldots, N, \ l = 1, \ldots, 5. \tag{18}$$

Accordingly, the compliance minimization problem Eq. (3) then becomes: find the design variables $\mathbf{E}, \mathbf{s}, \mathbf{w}$,

$$\min_{\mathbf{E},\mathbf{s},\mathbf{w}} \sum_{e=1}^{N}\sum_{l=1}^{5} w_{el}, \quad s.t. \tag{19}$$

$$\begin{cases} w_{el} + E_e \geq \left\| \begin{bmatrix} w_{el} - E_e \\ \sqrt{2/a_{el}}s_{el} \end{bmatrix} \right\|, \ 1 \leq e \leq N, 1 \leq l \leq 5, \\ \sum_{e=1}^{N}\sum_{l=1}^{5} s_{el}\mathbf{b}_{el} = \mathbf{f}, \\ \sum_{e=1}^{N} E_e \leq m_f T_0, \\ \underline{E_e} \leq E_e \leq \overline{E_e}, \ 1 \leq e \leq N, \end{cases} \tag{20}$$

where $\mathbf{E}$ is the vector of Young's modulus, $\mathbf{s} = \{s_{el}, \ 1 \leq e \leq N, 1 \leq l \leq 5\}$, $\mathbf{w} = \{w_{el}, \ 1 \leq e \leq N, 1 \leq l \leq 5\}$ are continuous design variables, T_0 is the reference global Young's modulus, m_f is the material cost fraction, and E_e is bounded by the prescribed values $\underline{E_e}, \overline{E_e}$. This gives an SOCP problem that is ready to solve.

4.2. Young's modulus $\mathbf{E}$ and Poisson's ratios $\boldsymbol{\nu}$ as design variables

Formulating the problem (3) as an SOCP when both $\mathbf{E}$ and $\boldsymbol{\nu}$ are design variables is more challenging, and we achieve this via introducing a novel bijection ϕ that maps the coefficients of Young's modulus and Poisson's ratio in Eq. (11) as two new independent variables. The details are explained below.

Consider the following bijection $\phi : (E, \nu) \to (P, Q)$

$$(P, \ Q) = \phi(E, \ \nu) = \left(\frac{E}{4(1+\nu)}, \ \frac{E}{8(1-\nu)}\right), \tag{21}$$

where $E > 0$, $-1 < \nu < 0.5$.

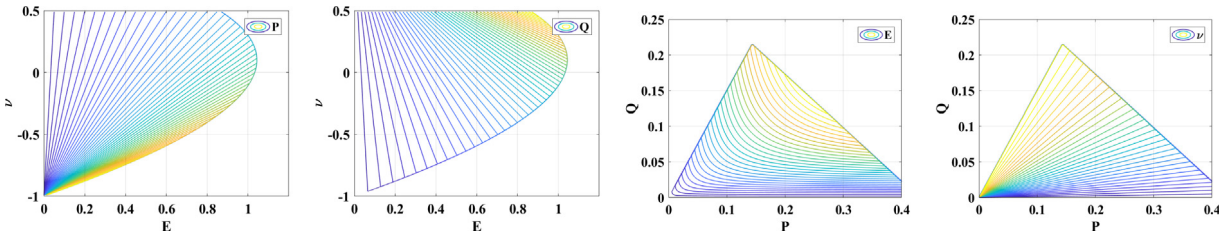

(a) P of (E, ν). (b) Q of (E, ν). (c) E of (P, Q). (d) ν of (P, Q).

Fig. 2. Plots of the proposed bijection $\phi : (E, \nu) \to (P, Q)$: $(P,\ Q) = \phi(E,\ \nu) = \left(\frac{E}{4(1+\nu)},\ \frac{E}{8(1-\nu)} \right)$ where $E > 0$, $-1 < \nu < 0.5$, as determined by classical elastic mechanics. And $\phi^{-1} : (P,\ Q) \to (E, \nu)$: $(E,\ \nu) = \phi^{-1}(P, Q) = \left(\frac{16PQ}{2Q+P},\ \frac{2Q-P}{2Q+P} \right)$. with $P > 0$, $Q > 0$, and $\frac{3}{2}P - Q > 0$.

This way, we have $\phi^{-1} : (P,\ Q) \to (E, \nu)$ defined by

$$(E,\ \nu) = \phi^{-1}(P, Q) = \left(\frac{16PQ}{2Q+P},\ \frac{2Q-P}{2Q+P} \right) \tag{22}$$

with $P > 0$, $Q > 0$, and $\frac{3}{2}P - Q > 0$.

Fig. 2 plots the mappings ϕ and ϕ^{-1} for an illustration. The feasible regions of (E, ν) and of (P, Q) are also respectively shown in 3 for an illustration. As we can see, the nonlinear transformation maps a curved domain into a polygon.

Substituting Eq. (22) into Eq. (11) gives

$$k_{e1} = k_{e2} = \frac{1}{3}P_e + \frac{1}{3}Q_e,\ \ k_{e3} = k_{e4} = P_e,\ \ k_{e5} = Q_e. \tag{23}$$

Owing to this transformation, instead of the nonlinear relationship of (E, ν) in Eq. (11), a linear formulation is constructed based on the new pair of design variables (P, Q).

In order to give a straightforward SOCP formulation and an optimization of higher computational efficiency, the five-item representation in Eq. (23) is further reformulated as a problem of seven variables based on Eqs. (9) and (10), which writes

$$K_e = \sum_{l=1}^{7} k_{e,l}^{P,Q} \mathbf{b}_{el}^{P,Q} \mathbf{b}_{el}^{P,Q\,T}, \tag{24}$$

where

$$k_{e1}^{P,Q} = k_{e2}^{P,Q} = \frac{1}{3}P_e, \quad k_{e3}^{P,Q} = k_{e4}^{P,Q} = P_e,$$

$$k_{e5}^{P,Q} = Q_e, \quad k_{e6}^{P,Q} = k_{e7}^{P,Q} = \frac{1}{3}Q_e,$$

and

$$\begin{aligned} \mathbf{b}^{P,Q} &= [\mathbf{b}_{e1},\ \mathbf{b}_{e2},\ \mathbf{b}_{e3},\ \mathbf{b}_{e4},\ \mathbf{b}_{e5},\ \mathbf{b}_{e1},\ \mathbf{b}_{e2}] \\ &= [\mathbf{b}_{e1}^{P,Q},\ \mathbf{b}_{e2}^{P,Q},\ \mathbf{b}_{e3}^{P,Q},\ \mathbf{b}_{e4}^{P,Q},\ \mathbf{b}_{e5}^{P,Q},\ \mathbf{b}_{e6}^{P,Q},\ \mathbf{b}_{e7}^{P,Q}]. \end{aligned} \tag{25}$$

Accordingly, the trace constraints in (3) are derived

$$\mathrm{Tr}(\mathbf{D}_e) = \frac{E_e(5-\nu_e)}{2(1+\nu_e)(1-\nu_e)} = 8Q_e + 6P_e, \tag{26}$$

$$T = \sum_{e=1}^{N} \mathrm{Tr}(\mathbf{D}_e) = \sum_{e=1}^{N} (8Q_e + 6P_e). \tag{27}$$

Poisson's constraint $\underline{\nu_e} \le \nu_e \le \overline{\nu_e}$ becomes

$$\begin{cases} 2(\overline{\nu_e} - 1)Q_e + (\overline{\nu_e} + 1)P_e \ge 0 \\ 2(\underline{\nu_e} - 1)Q_e + (\underline{\nu_e} + 1)P_e \le 0 \end{cases} \tag{28}$$

As we comment after Eq. (14), the inferior of the problem is equal to the structural compliance. Thus, the objective of minimizing the compliance c can instead be achieved by minimizing $\sum_{l=1}^{7} w_{el}$ at the constraint specified in Eq. (14). Introducing the key observation, the optimization problem (3) is rewritten in an SOCP: find the design variables P_e, Q_e, s_{el}, w_{el}

$$\begin{aligned}
&\min \quad 2\sum_{e=1}^{N}\sum_{l=1}^{7} w_{el} \\
&s.t. \\
&(a.1) \quad w_{e1} + P_e \ge \left\| \begin{bmatrix} w_{e1} - P_e \\ \sqrt{6}\, s_{e1} \end{bmatrix} \right\| \\
&(a.2) \quad w_{e2} + P_e \ge \left\| \begin{bmatrix} w_{e2} - P_e \\ \sqrt{6}\, s_{e2} \end{bmatrix} \right\| \\
&(a.3) \quad w_{e3} + P_e \ge \left\| \begin{bmatrix} w_{e3} - P_e \\ \sqrt{2}\, s_{e3} \end{bmatrix} \right\| \\
&(a.4) \quad w_{e4} + P_e \ge \left\| \begin{bmatrix} w_{e4} - P_e \\ \sqrt{2}\, s_{e4} \end{bmatrix} \right\| \\
&(a.5) \quad w_{e5} + Q_e \ge \left\| \begin{bmatrix} w_{e5} - Q_e \\ \sqrt{2}\, s_{e5} \end{bmatrix} \right\| \\
&(a.6) \quad w_{e6} + Q_e \ge \left\| \begin{bmatrix} w_{e6} - Q_e \\ \sqrt{6}\, s_{e6} \end{bmatrix} \right\| \\
&(a.7) \quad w_{e7} + Q_e \ge \left\| \begin{bmatrix} w_{e7} - Q_e \\ \sqrt{6}\, s_{e7} \end{bmatrix} \right\| \\
&\qquad (e = 1, \ldots, N) \\
&(b) \quad \sum_{e=1}^{N}\sum_{l=1}^{7} s_{el}\mathbf{b}_l = \mathbf{f} \\
&(c) \quad \sum_{e=1}^{N} (8Q_e + 6P_e) \le \overline{T} \\
&(d.1) \quad P_e > 0, \\
&(d.2) \quad Q_e > 0, \\
&(d.3) \quad \frac{3}{2}P_e - Q_e > 0, \\
&\qquad (e = 1, \ldots, N) \\
&(e.1) \quad 8Q_e + 6P_e \le \overline{T_e}, \\
&(e.2) \quad 8Q_e + 6P_e \ge \underline{T_e}, \\
&\qquad (e = 1, \ldots, N) \\
&(f.1) \quad 2(\overline{\nu_e} - 1)Q_e + (\overline{\nu_e} + 1)P_e \ge 0 \\
&(f.2) \quad 2(\underline{\nu_e} - 1)Q_e + (\underline{\nu_e} + 1)P_e \le 0 \\
&\qquad (e = 1, \ldots, N).
\end{aligned} \tag{29}$$

Global optimum of the SOCP is ready to solve. Once the optimized solution $\{(P_e, Q_e)\}$ is obtained, the material distribution of Young's modulus and Poisson's ratio can be derived from the mapping $\phi^{-1} : (P,\ Q) \to (E, \nu)$ directly. The unique mapping between (E, ν) and (P, Q) spaces ensures that a global optimal solution in terms of (E, ν) can always be obtained.

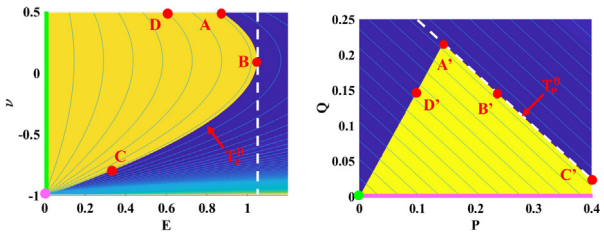

(a) Material tensor space (E, ν). (b) SOCP solution space (P, Q).

Fig. 3. Mapping between two feasible regions in two different design spaces, where the curved isocontour is mapped straight-lines. A(0.86, 0.50), B(1.04, 0.10), C(0.33, −0.80), D(0.60, 0.50). A′(0.14, 0.22), B′(0.24, 0.15), C′(0.40, 0.02), D′(0.10, 0.15).

Extending the proposed method to problems defined on other types of mesh elements mainly depends on the decomposition form of (12). It works well on 2D or 3D regular grids, specifically 2D square elements and regular triangle, 3D cubic elements and regular tetrahedral elements. Its extension to other types of general mesh elements are non-trivial.

5. Material space reduction via material clustering

The derived material distribution from the FIMO is almost different everywhere within the design domain. The great number of material types is to be reduced to a prescribed number as small as 2 via clustering techniques as studied here. The challenge of applying the well-studied clustering techniques here is to maintain high compliance fidelity of the generated structures. Performing the hierarchical clustering method in the intermediate (P, Q) space demonstrates nice performance on numerical examples, and is finally adopted.

Hierarchical clustering groups data over a variety of scales by creating a cluster tree or dendrogram. The tree is not a single set of clusters, but rather a multilevel hierarchy, where clusters at one level are joined as clusters at the next level. In the proposed approach, the similarity between two material tensors is tested via various different measures, and is ultimately defined by the Euclidean distance in the (P, Q) space. Based on this proximity, different design elements are iteratively grouped into a binary, hierarchical cluster tree. The final k-clusters are derived via cutting the hierarchical tree into k clusters, and the corresponding cluster center is decided by averaging the values of (P, Q)'s in each cluster. Since the global and local material constraints are all linear with respect to the design variables P and Q, they will be preserved perfectly after clustering.

A nice property of the proposed clustering algorithm lies in fact that the global trace constraint can be accurately preserved within the clustering process, as further explained below. Suppose the global trace of a continuous FIMO solution is T^{con}, according to (27), that is,

$$T^{con} = \sum_{e=1}^{N} \mathrm{Tr}(\mathbf{D}_e^{con}) = \sum_{e=1}^{N} (8Q_e^{con} + 6P_e^{con}), \tag{30}$$

where N is the number of design element, and (P_e^{con}, Q_e^{con}) are the associated material parameters to an element e.

Suppose the N kinds of continuous materials are grouped into k discrete clusters as Ξ_i, $i = 1, \ldots, k$. According to the proposed clustering strategy, the material parameters in (P, Q) space of each new cluster are defined by

$$P_i^{clu} = \frac{1}{|\Xi_i|} \sum_{e \in \Xi_i} P_e^{con}, \quad Q_i^{clu} = \frac{1}{|\Xi_i|} \sum_{e \in \Xi_i} Q_e^{con}, \quad i = 1, \ldots, k. \tag{31}$$

Accordingly, the clustered material parameters (P_e^{dis}, Q_e^{dis}) for each element $e \in \Xi_i$ are determined $(P_e^{dis}, Q_e^{dis}) = (P_i^{clu}, Q_i^{clu})$. Consequently, the global trace of the new material distribution after clustering is calculated as

$$\begin{aligned} T^{dis} &= \sum_{e=1}^{N} \mathrm{Tr}(\mathbf{D}_e^{dis}) \\ &= \sum_{e=1}^{N} (8Q_e^{dis} + 6P_e^{dis}) \\ &= \sum_{i=1}^{k} \sum_{e \in \Xi_i} (8Q_e^{dis} + 6P_e^{dis}) \\ &= \sum_{i=1}^{k} \sum_{e \in \Xi_i} (8Q_e^{clu} + 6P_e^{clu}) \\ &= \sum_{i=1}^{k} |\Xi_i| \cdot (8Q_e^{clu} + 6P_e^{clu}) \\ &= \sum_{i=1}^{k} \sum_{e \in \Xi_i} (8Q_e^{con} + 6P_e^{con}) \\ &= T^{con} \end{aligned} \tag{32}$$

which means the global trace constraint is accurately preserved.

We also test the performance of K-means clustering at various similarity measure. K-means is the classical clustering approaches aiming to partition n observations into k clusters in which each observation belongs to the cluster with the nearest mean, which ultimately results in a set of Voronoi cells. In the K-mean approach, the final clustering depends heavily on the initial cluster seeds distribution generated by the k−means++ algorithm. In practise, we select the best result that demonstrates the smallest structural compliance after acceptable times of repeating. More details on the performance of different material clustering approaches will be further explained in Section 6.

6. Numerical experiments

The proposed approach has been implemented in MATLAB R2017b, and run on a PC of Intel Core i7-9700 K of 3.6 GHz CPU and 32 GB RAM. The SOCP problems are solved by calling CPLEX 12.8.0 from MATLAB through YALMIP. Its performance is tested on various aspects using different examples of the same size 80×30 for ease of comparison. The first example in Section 6.1 is implemented to compare its effectivity in deriving optimized structure against those derived by the classic topology optimization, and the effect of Poisson's ratio. The second example in Section 6.2 tests its usage and performances in different load cases. The third example in Section 6.3 tests performance of the material clustering in terms of clustering number or algorithms. In the end, results on various other examples are further reported in Section 6.4. All the results of the classic topology optimization are obtained without using filter since no filter is considered in the proposed strategy for a fair comparison; the usage of filter actually has ignorable effect on the topology optimization target.

The following notations will be used throughout this section.

Material constraints. A material at Young's modulus E and Poisson's ratio is also called material (E, ν) for short. The material trace for each design element is constrained by

$$\Omega_{T_e}^0 = [0, T_e^0],$$

where T_e^0 is the trace of the material $(1, 0.3)$.

The examples were usually tested under different global material costs m_f ranging from 0.2 to 0.9 at a step of 0.1, and 0.95, denoted $m_f \in [0.2 : 0.1 : 0.9, 0.95]$ for short.

Table 1
Comparisons between different optimization approaches: SIMP-c from classical topology optimization setting *penal* = 1 and Poisson's ratio $\nu = 0.3$, the SOCP approach for different ranges of Poisson's ratios. The global volume constraint m_f, defined in (3), is varied from 0.2 to 0.95.

Method	SIMP-c	Ours						
m_f	ν							
	0.3	0.3	[0.1,0.4]		[−0.2,0.4]		[−0.99,0.49]	
0.20	256.23	256.04	236.73	7.54%	227.67	11.08%	219.47	14.28%
0.30	181.65	181.51	168.49	7.17%	162.68	10.37%	157.43	13.27%
0.40	145.51	145.44	135.52	6.82%	131.39	9.66%	127.73	12.18%
0.50	124.95	124.94	116.86	6.46%	113.78	8.93%	111.09	11.09%
0.60	112.29	112.25	105.37	6.13%	103.04	8.20%	101.07	9.96%
0.70	104.16	104.12	98.05	5.83%	96.29	7.52%	94.84	8.91%
0.80	98.93	98.90	93.38	5.58%	92.05	6.93%	91.05	7.94%
0.90	95.71	95.69	90.55	5.37%	89.54	6.43%	88.88	7.12%
0.95	94.71	94.71	89.68	5.31%	88.77	6.27%	88.27	6.80%

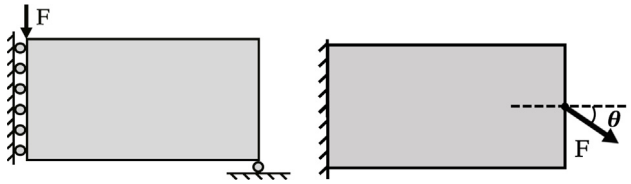

(a) Half MBB (b) Tension example

Fig. 4. Problem definitions.

Four different kinds of ranges Ω_ν of Poisson's ratio ν are used:

$$\Omega^a_{\nu_e} = [0.3], \quad \Omega^b_{\nu_e} = [0.1, 0.4],$$
$$\Omega^c_{\nu_e} = [-0.2, 0.4], \quad \Omega^d_{\nu_e} = [-0.99, 0.49], \tag{33}$$

satisfying $\Omega^a_{\nu_e} \subset \Omega^b_{\nu_e} \subset \Omega^c_{\nu_e} \subset \Omega^d_{\nu_e}$. Note that $\Omega^a_{\nu_e}$ is equivalent to a fixed Poisson's ratio of 0.3.

Benchmark. Two kinds of benchmarks are used in this section: numerical results computed with classical topology optimization approach SIMP [38] at a penalty power *penal* = 3, and its continuous version *penal* = 1, denoted SIMP-c. In both approaches, Young's modulus is allowed to vary within range $[E_{\min}, 1]$ ($E_{\min} = 0.1^3$), and Poisson's ratio is set 0.3.

Effectivity index. An effectivity index is defined to measure the relative compliance variation to two different optimized structures,

$$r = \frac{|c_1 - c_0|}{c_0}, \tag{34}$$

where c_0 and c_1 are compliances of the two results.

In our experiments, the computation costs come from two main tasks: assembling SOCP constraints in MATLAB taking about 30 s, and calling CPLEX to solve the associated SOCP taking about 50∼60 s. A future code improvement is expected to further improve the computational efficiency .

6.1. Overall performance in continuous material space

Effectivity of the FIMO solution in deriving optimal solution is first tested and compared with those derived by the classic topology optimization, under different cases for $m_f \in [0.2 : 0.1 : 0.9, 0.95]$, and $\nu \in \Omega_{\nu_e}$ as defined in Eq. (33). The numerical results are summarized in Table 1 and plotted in Fig. 5. The two different cases of having or not Poisson's ratio as design variables are respectively studied below.

6.1.1. Optimization of young's modulus

The test studies the degenerated case that only Young's modulus is taken as design variable, which corresponds to the case $\nu \in \Omega^a_{\nu_e} = [0.3]$. The obtained results are shown in the third column in Table 1, in comparison with SIMP-c in the second column. The two results demonstrate very high compliance consistency, and the proposed is always slightly better in having a smaller compliance. The phenomenon may be explained from the fact that a minimum value of Young's modulus $E_{\min}$ is used in SIMP-c to avoid the singularity case caused by void element while the proposed does not need such special handling. The result on the other hand also shows the global convergence of SIMP-c. The obtained material distributions are also shown on the top of Fig. 5 for illustration.

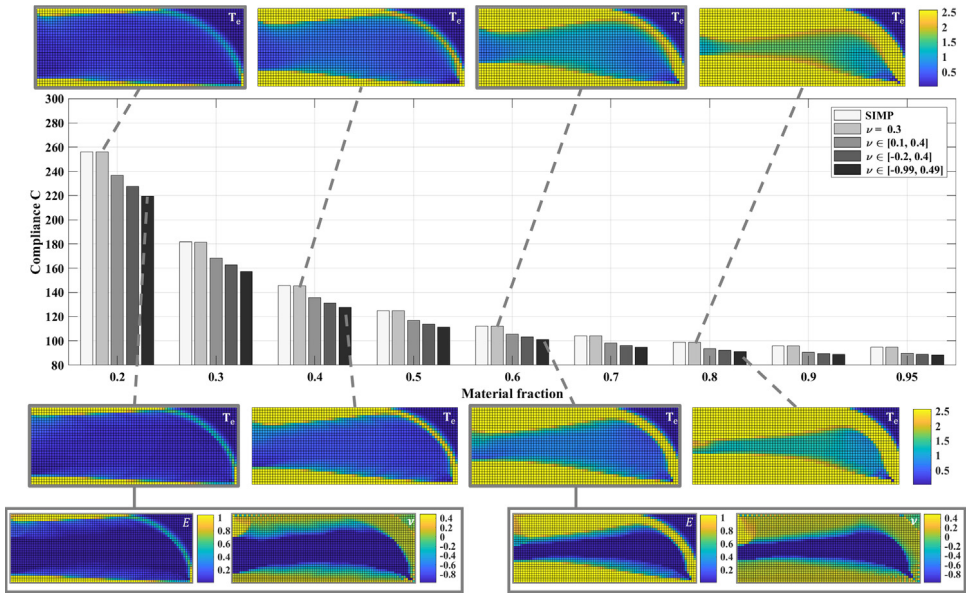

Fig. 5. Performance of the approach at constraints of different ranges of Poisson's ratios. Introducing Poisson's ratio into design always results in a better structure of smaller compliance than those obtained via using single variable of Young's modulus. The top and bottom figures show distributions of the traces of material tensors of the resulted solutions. Similar trace distributions are observed despite of different ranges of Poisson's ratios.

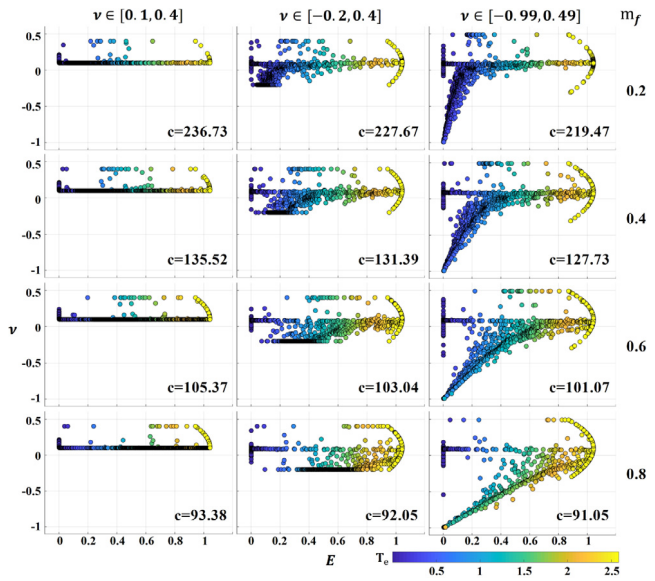

Fig. 6. Material solution distributions at different constraints of ranges of Poisson's ratios or material cost m_f. Each point represents an optimized elemental material tensor in (E, ν) space, colored by the value of trace $\mathrm{Tr}(\mathbf{D}_e(E, \nu))$.

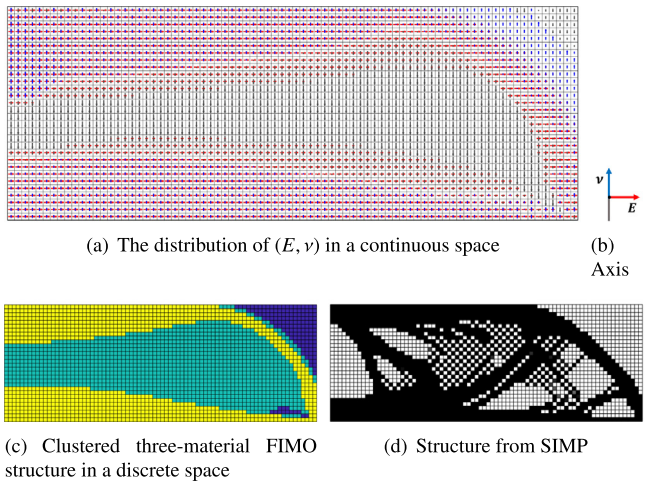

(a) The distribution of (E, ν) in a continuous space (b) Axis

(c) Clustered three-material FIMO structure in a discrete space (d) Structure from SIMP

Fig. 7. The specific distribution of Young's modulus and Poisson's ratio for the optimized structure generated at $m_f = 0.6$ and $\Omega^d_{\nu_e} = [-0.99, 0.49]$ is given in (a), (c) gives the derived three-material FIMO structure as compared with structure from classical SIMP in (d). In (c) the elements in yellow indicate the stiffest material, the blue the softest, and the green in between them. . (For interpretation of the references to color in this figure legend, the reader is referred to the web version of this article.)

6.1.2. Optimization of both Young's modulus and Poisson's ratio

The performance is tested at different ranges of Poisson's ratios, as depicted in Eq. (33), and summarized in Table 1 and compared in Figs. 5 and 6. As can be observed from the results, introducing Poisson's ratio into design always results in a better structure of smaller compliance than those obtained via only taking Young's modulus as design variable. We also observe that the larger range Poisson's ratio lies in, the better structure it produces, which is consistent with our intuition. In addition, more performance improvement was observed for a smaller global material constraint m_f, with effectivity indices ranging from 5% to 15%. It is also interesting to note in Fig. 5 that the trace T_e distributions at different ranges of Poisson ratios have close shape similarity despite of the different distributions of Poisson's ratios, demonstrating the approach's stability and the importance of the material trace.

The distributions of material solution are also plotted in Fig. 6 in the plane of Poisson's ratio and Young's modulus within range, where elements of negative Poisson's ratios are widely observed. It also shows the usage and effective NPR material in design.

We also plot in Fig. 7 values of Young's modulus and Poisson's ratio within the design domain for the solution at $m_f = 0.6$ and $\Omega^d_{\nu_e} = [-0.99, 0.49]$, where Young's modulus, positive and negative Poisson's ratio are represented by red, blue and gray arrows, scaled by their absolute values. The results are also compared with those obtained via SIMP and the clustered three-material structure in Fig. 7(c,d). It is very interesting to note that the stiffest elements of the three structures, respectively elements in red, yellow and black in Fig. 7(a),(b),(c), are located similarly. However, the optimized structure generated from SIMP has many

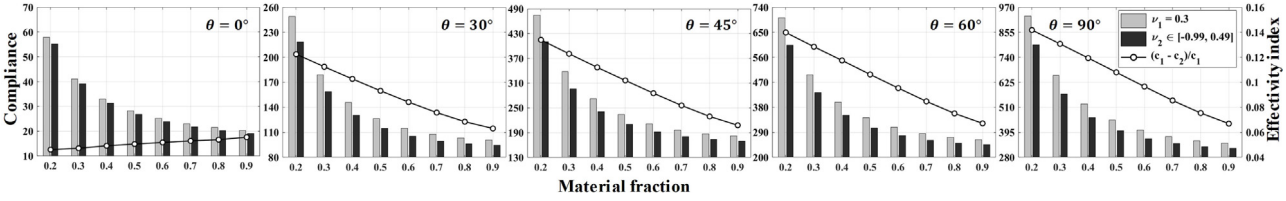

Fig. 8. The compliances and effectivity indices of the tension problem for different load orientations $\theta = 0°, 30°, 45°, 60°, 90°$ under different values of material costs m_f.

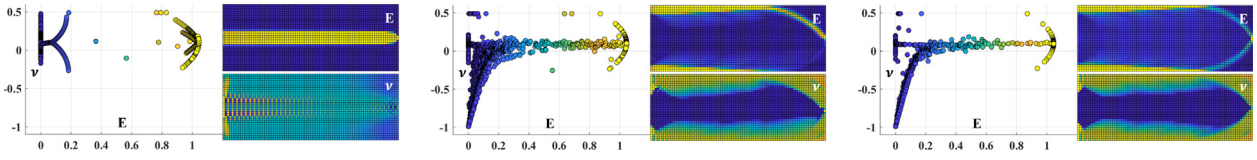

(a) $\theta = 0°$ (b) $\theta = 45°$ (c) $\theta = 90°$

Fig. 9. The optimized material distribution of the tension problem for different load orientations $\theta = 0°, 45°, 90°$ and values of material costs $m_f = 0.2$. In each subfigure, the left shows the solution material distributions, and the right gives distribution of Young's modulus and Poisson's ratio in the design domain.

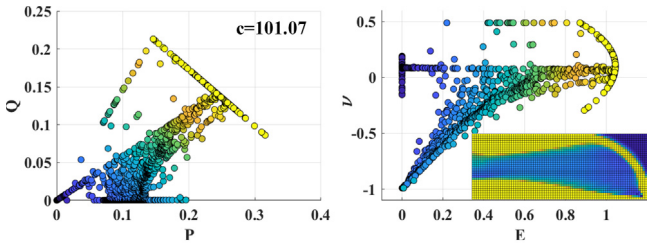

(a) Continuous result, $c = 101.07$.

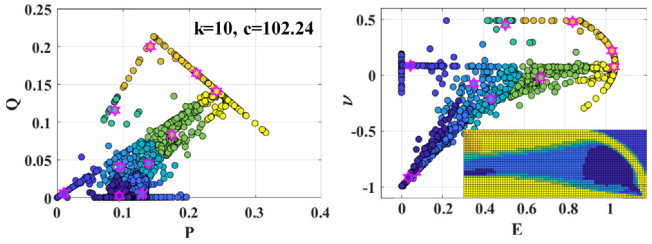

(b) Discrete result, $c = 102.24$.

Fig. 10. The specific continuous and discrete material distributions of the half MBB problem in (P, Q), (E, ν) space, and their trace structures. The material fraction $m_f = 0.6$, and the target cluster number is set 10. (For interpretation of the references to color in this figure legend, the reader is referred to the web version of this article.)

interior support details to withstand the external loads while the optimized FIMO structure seems to utilize elements of negative Poisson's ratio to withstand the external loads.

6.2. Performance of optimizing (E, ν) in different load cases

We test here the effect of the FIMO concept in improving structural performance for the tension example in Fig. 4(b) at five different load orientations: $\theta \in \{0°, 30°, 45°, 60°, 90°\}$, where material constraint $m_f = 0.2$, Poisson's ratio range is set by $\Omega_{\nu_e}^d = [-0.99, 0.49]$. The results are summarized in Table 2 and in Fig. 8 in comparison with SIMP-c, or case $\nu = 0.3$. The material distributions within the design domain and the $E - \nu$ space are also shown in Fig. 9.

As we can see from the results, in case that the angle $\theta \neq 0$, the introduction of Poisson ratio much improves the structural compliance at a maximal effective index of 14.18%. On the other hand, when $\theta = 0$ the effectivity index has a maximal value of 5.52%. Furthermore, when $\theta \neq 0$ the effectivity index generally tends to become larger as the material cost constraint m_f becomes smaller. The case $\theta \neq 0$ has a vice versa performance. The interesting phenomenon may be explained from the observation that the element materials are much dispersive along the axis of Poisson's ratio when $\theta \neq 0$, as indicated in Fig. 9.

6.3. Material clustering

This section tests the effect of the proposed material clustering technique using the half MBB problem in Fig. 4(a), respectively the overall performance, cases of different cluster numbers, and cases of different clustering techniques.

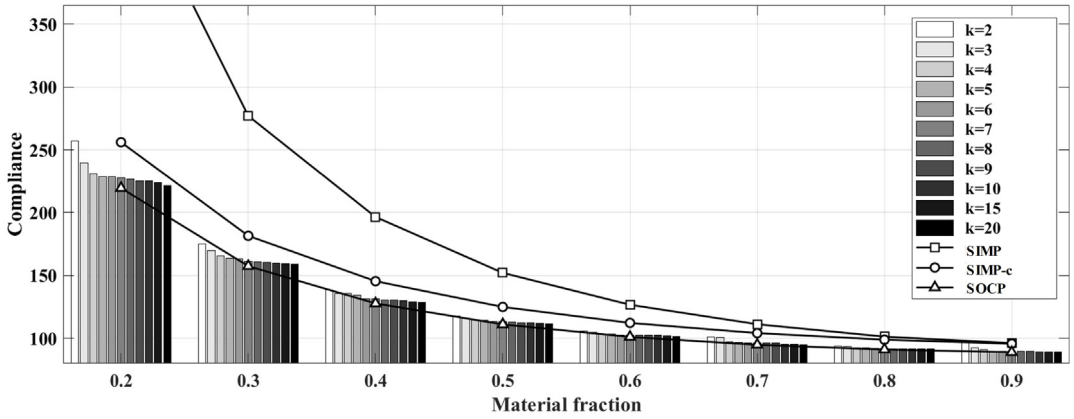

(a) Compliance.

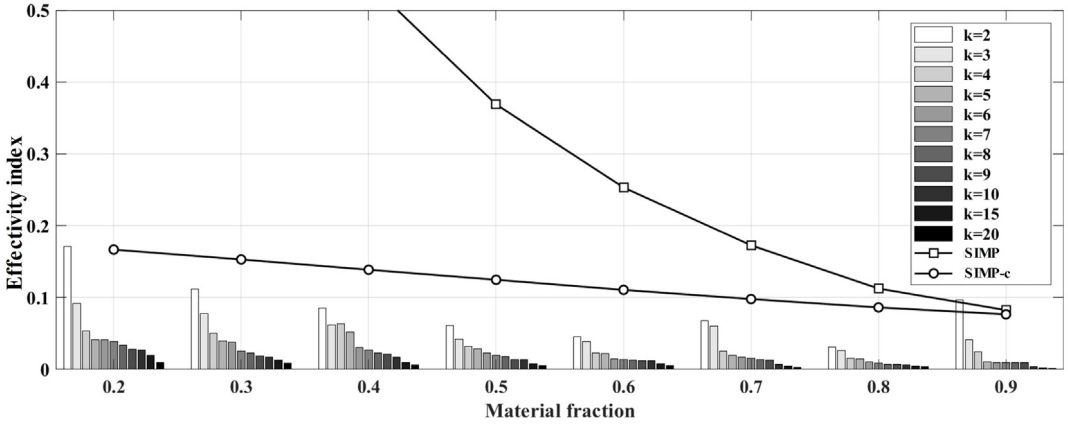

(b) Effectivity index.

Fig. 11. Performance of the proposed hierarchical material clustering algorithm at different clustering numbers k and material cost fraction m_f. They are compared with benchmark results obtained from classical topology optimization approach SIMP and its continuous version SIMP-c. Here, the Effectivity index is defined in Eq. (34), and the reference value c_0 refers to the SOCP results.

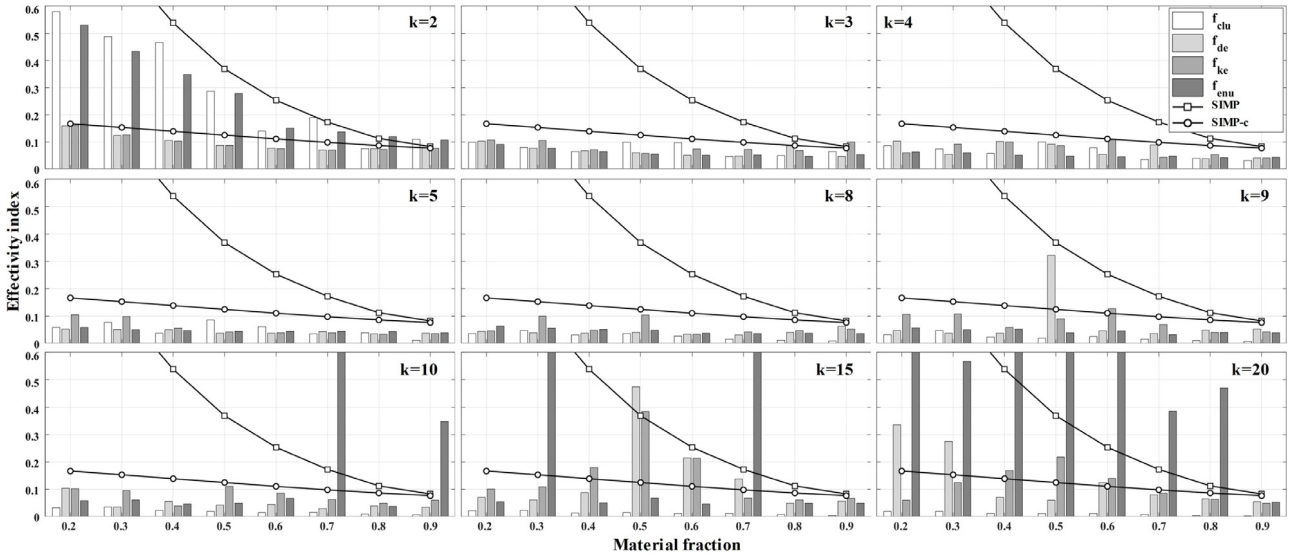

Fig. 12. Effectivity indices of other four clustering algorithms, tested at different cluster number k and material cost fraction m_f. Results of the benchmark SIMP and SIMP-c are shown by lines for references.

Table 2
Effectivity indices of the tension problem optimized under different load orientations Ω_{v_e} and values of material costs θ.

m_f	θ				
	0°	30°	45°	60°	90°
0.20	4.51%	12.24%	13.49%	13.99%	14.18%
0.30	4.62%	11.24%	12.36%	12.84%	13.07%
0.40	4.82%	10.28%	11.27%	11.75%	11.93%
0.50	4.97%	9.32%	10.22%	10.63%	10.80%
0.60	5.10%	8.42%	9.18%	9.54%	9.66%
0.70	5.22%	7.58%	8.20%	8.48%	8.55%
0.80	5.32%	6.85%	7.30%	7.51%	7.54%
0.90	5.52%	6.30%	6.59%	6.71%	6.69%

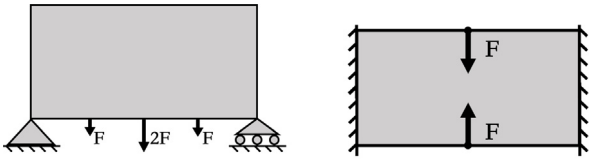

(a) Bridge (b) A new example

Fig. 13. Problem definition.

6.3.1. Overall performance

As explained in Section 5, dimension of the material space can be reduced to a specified number via a hierarchical clustering in the (P, Q) space. The result is first shown in Fig. 10 for a material fraction $m_f = 0.6$, Poisson's ratio range $\Omega^d_{v_e} = [-0.99, 0.49]$, and a target cluster number 10.

Fig. 10(a) shows the results in the continuous case, respectively in (P, Q) and (E, ν) spaces, where material point color indicates the trace value. The derived multi-material solution is shown in Fig. 10(b) both in (P, Q) and (E, ν). The cluster center of each group is highlighted in pink. The target compliance is increasing slightly from 101.07 to 102.24 before and after clustering, demonstrating high physical fidelity. As can also be observed from Fig. 10(b), the clustered groups are pretty dispersive in the (P, Q) space but not in the (E, ν) space, where material points close to each other may belong to different cluster groups. This demonstrates the effectivity and importance of conducting clustering in the (P, Q) space instead of in the (E, ν) space.

6.3.2. Effect of different clustering numbers

Performance of the approach is also tested at different clustering numbers $2 \sim 10$, 15 and 20, a material fraction $m_f = 0.6$, Poisson's ratio range $\Omega^d_{v_e} = [-0.99, 0.49]$. They are also compared with benchmark results of SIMP, SIMP-c, and the continuous SOCP results. The results are summarized in Fig. 11.

The clustered multi-material structures always demonstrate close approximation to the SOCP solutions in all the cases, which always tends to become better as the clustering number increases. In addition, the resulted multi-material structures always have a smaller (thus better) compliance than those obtained via SIMP-c or SIMP, even at the simplest case of using 2 clusters. Such ideally nice phenomenon is hard to achieve using other clustering approach as we will see later. The nice phenomenon can also be observed from plots of the effectivity indices in Fig. 11(b), where the proposed FIMO clusters always have smaller value than the other two reference approaches. The phenomenon becomes clearer when the volume constraint becomes smaller and the number of clusters becomes larger.

6.3.3. Effectivity of different clustering approaches

Four different clustering approaches were tested, each at a cluster number $k = 2, 3, 4, 5, 8, 9, 10, 15, 20$, including the agglomerative hierarchical clustering method in (E, ν) space, denoted $f_{hc/(E,\nu)}$, and the K-means clustering under different distance measurements: the Euclidean distance of elasticity matrix $\mathbf{D}_e$, of stiffness matrix $\mathbf{K}_e$, and of (E, ν), respectively denoted $f_{km/De}$, $f_{km/Ke}$ and $f_{km/(E,\nu)}$. The results are also compared with the benchmark SIMP and SIMP-c results, and shown in Fig. 12. Note here the higher the index, the worse the approach.

Looking through the nigh subgraphs in Fig. 12, none of the four approaches are stable and acceptable for all material fractions and different number of clusters. They may even have a much larger value of effectivity indices than those of SIMP-c or SIMP. In contrast, the proposed hierarchical clustering in (P, Q) space is always effective and stable, as has been explained in Section 6.3.2.

In addition, experiments show that the K-means approach usually has difficulty in convergence and the results strongly depend on the initial seeds. In particular, it becomes increasingly unstable and unreliable as k becomes larger. The above results take the best amongst 20-times experiments.

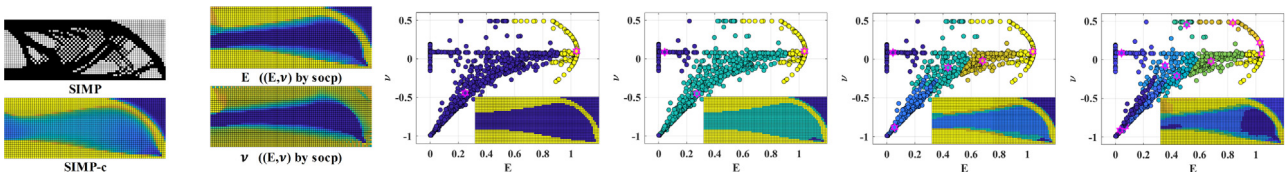

(a) c_{SIMP} = 126.67, c_{SIMP-c} = 112.25. (b) c = 101.07. (c) k = 2, c = 105.68. (d) k = 3, c = 104.98. (e) k = 5, c = 103.26. (f) k = 10, c = 102.24.

Fig. 14. Results of half MBB in Fig. 4(a): SIMP, SIMP-c, optimizing (E, ν) by SOCP, and discrete structures for different cluster numbers k, $m_f = 0.6$.

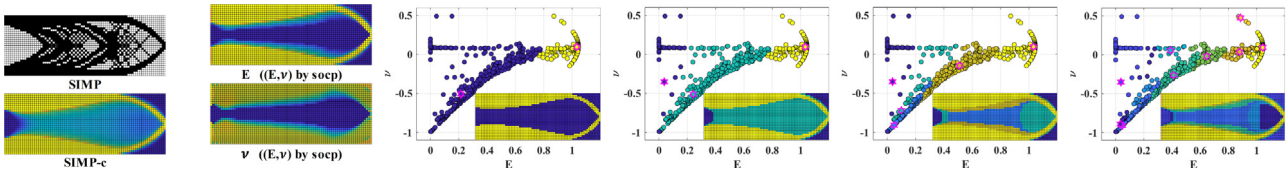

(a) c_{SIMP} = 451.47, c_{SIMP-c} = 404.81. (b) c = 365.69. (c) k = 2, c = 379.32. (d) k = 3, c = 376.45. (e) k = 5, c = 371.45. (f) k = 10, c = 367.87.

Fig. 15. Results of tension example in Fig. 4(b) of load orientation $\theta = 90°$: SIMP, SIMP-c, optimizing (E, ν) by SOCP, and discrete structures for different cluster numbers k, $m_f = 0.6$.

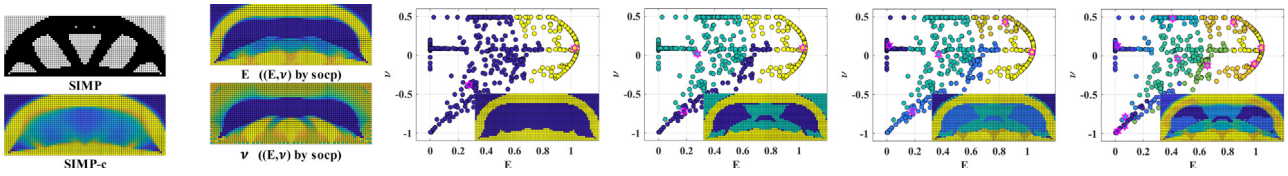

(a) c_{SIMP} = 184.61, c_{SIMP-c} = 171.60. (b) c = 152.65. (c) k = 2, c = 166.62. (d) k = 3, c = 164.21. (e) k = 5, c = 161.01. (f) k = 10, c = 156.83.

Fig. 16. Results of bridge example in Fig. 13(a): SIMP, SIMP-c, optimizing (E, ν) by SOCP, and discrete structures for different cluster numbers k, $m_f = 0.6$.

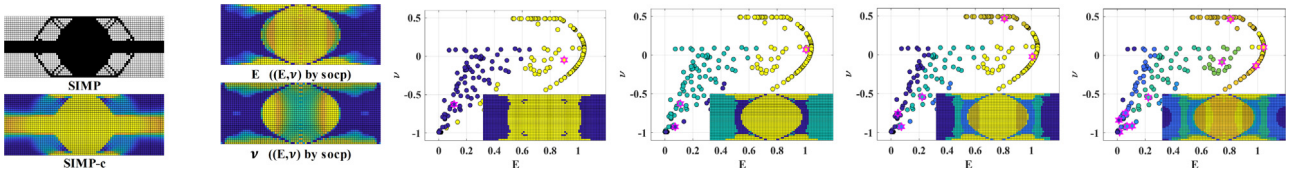

(a) c_{SIMP} = 5.61, c_{SIMP-c} = 5.58. (b) = 5.18. (c) k = 2, c = 6.02. (d) k = 3, c = 5.47. (e) k = 5, c = 5.40. (f) k = 10, c = 5.22.

Fig. 17. Results of the problem in Fig. 13(b): SIMP, SIMP-c, optimizing (E, ν) by SOCP, and discrete structures for different cluster numbers k, $m_f = 0.6$.

6.4. Other examples

The approach's performance was also tested for various other examples: the half MBB in Fig. 4(a), the bridge in Fig. 13(a), the tension example of $\theta = 90°$ in Fig. 4(b) and the example of opposite loads in Fig. 13(b). All the four examples are under the same global material constraint $m_f = 0.6$ and Poisson's ratio range $\Omega^d_{\nu_e} = [-0.99, 0.49]$. Their numerical results are shown in Figs. 14–17, including cases of SIMP, SIMP-c, the proposed FIMO via SOCP, and the clustered results at a cluster number $k = 2, 3, 5, 10$. Specific target compliance values are also given below each subgraph. The proposed approach is very stable and effective for all the tests in always achieving better design target values, and high-fidelity discrete structures .

7. Conclusion

The study proposes a novel method solving a new structural design problem FIMO by simultaneously optimizing Young's modulus and Poisson's ratio within a design domain. Based on the proposed formulation of SOCP, global optimum is theoretically achievable and the challenging singularity issue on void elements is also avoided. Meanwhile, a discrete material clustering algorithm is developed to reduce the material dimension of the resulted structure to any prescribed number, which shows close performance fidelity to the continuous case. Performance of the approach was tested on various 2D numerical examples demonstrating that the approach can always achieve structures of decent performances, using a reference result obtained via

topology optimization, and demonstrating the high effectivity of introducing (negative) Poisson's ratio in structural design.

The present method is mainly limited to the computation cost of the MATLAB code in assembling the SOCP constraints by YALMIP and calling for CPLEX for high resolution problems, which is to be optimized in our future study. In addition, an effective approach to designing micro-structures of target material tensors (isotropic or not) is very desirable so that the derived optimal structures could be ultimately put into manufacturing. Further extending the study to discrete structural designs or to handle cases of large deformations and stress constraints also deserves further research efforts.

Acknowledgments

The work described in this paper is partially supported by the NSFC of China (Nos. 61872320, 61472356), and the National Key Research and Development Program of China (No. 2018YFB1700603).

References

[1] Bendsoe M. Optimization of structural topology, shape, and material. Springer Berlin Heidelberg; 1995.
[2] Sigmund O, Maute K. Topology optimization approaches: a comparative review. Struct Multidiscip Optim 2013;48(6):1031–55.
[3] van Dijk NP, Maute K, Langelaar M, van Keulen F. Level-set methods for structural topology optimization: a review. Struct Multidiscip Optim 2013;48(3):437–72.
[4] Xia L, Xia Q, Huang X, Xie YM. Bi-directional evolutionary structural optimization on advanced structures and materials: A comprehensive review. Arch Comput Methods Eng 2016;1–42.
[5] Wu J, Dick C, Westermann R. A system for high-resolution topology optimization. IEEE Trans Vis Comput Graphics 2016;22(3):1195–208.
[6] Clausen A, Wang F, Jensen JS, Sigmund O, Lewis JA. Topology optimized architectures with programmable Poisson's ratio over large deformations. Adv Mater 2015;27(37):5523–7.
[7] Niemann S, Kolesnikov B, Hühne C, Querin O, Toropov V. The use of topology optimisation in the conceptual design of a next generation lattice composite fuselage structure. In: Aircraft structural design conference. 2012.
[8] Zhu JH, Zhang WH, Xia L. Topology optimization in aircraft and aerospace structures design. Arch Comput Methods Eng 2015;1–28.
[9] Qian X. Topology optimization in B-spline space. Comput Methods Appl Mech Engrg 2013;265:15–35.
[10] Xu G, Zhang W, Jian Z, Jie Y. Explicit structural topology optimization based on moving morphable components (MMC) with curved skeletons. Comput Methods Appl Mech Eng 2016;310:711–48.
[11] Olson GB. Designing a new material world. Science 2000;288(5468):993–8.
[12] Deng J, Yan J, Cheng G. Multi-objective concurrent topology optimization of thermoelastic structures composed of homogeneous porous material. Struct Multidiscip Optim 2013;47(4):583–97.
[13] Xia L, Breitkopf P. A reduced multiscale model for nonlinear structural topology optimization. Comput Methods Appl Mech Engrg 2014;280:117–34.
[14] Xia L, Breitkopf P. Multiscale structural topology optimization with an approximate constitutive model for local material microstructure. Comput Methods Appl Mech Engrg 2015;286:147–67.
[15] Lieu QX, Lee J. A multi-resolution approach for multi-material topology optimization based on isogeometric analysis. Comput Methods Appl Mech Engrg 2017;323:272–302.
[16] Panetta J, Zhou Q, Malomo L, Pietroni N, Cignoni P, Zorin D. Elastic textures for additive fabrication. ACM Trans Graph 2015;34(4):135:1–135:12.
[17] Schumacher C, Bickel B, Rys J, Marschner S, Daraio C, Gross M. Microstructures to control elasticity in 3D printing. ACM Trans Graph 2015;34(4):136:1–136:13.
[18] Kocvara M, Stingl M, Zowe J. Free material optimization: recent progress. Optimization 2008;57(1):79–100.
[19] Kocvara M, Nesterov Y, Xia Y. A subgradient method for free material design. SIAM J Optim 2016;26(4):2314–54.
[20] Liu B, Feng X, Zhang SM. The effective Young's modulus of composites beyond the voigt estimation due to the Poisson effect. Compos Sci Technol 2009;69(13):2198–204.
[21] Kocer C, Mckenzie DR, Bilek MM. Elastic properties of a material composed of alternating layers of negative and positive Poisson's ratio. Mater Sci Eng A 2009;505(1):111–5.
[22] Zuo ZH, Xie YM. Maximizing the effective stiffness of laminate composite materials. Comput Mater Sci 2014;83(2):57–63.
[23] Shufrin I, Pasternak E, Dyskin AV. Hybrid materials with negative Poisson's ratio inclusions. Internat J Engrg Sci 2015;89:100–20.
[24] Long K, Yuan PF, Xu S, Xie YM. Concurrent topological design of composite structures and materials containing multiple phases of distinct Poisson's ratios. Eng Optim 2017;(4):1–16.
[25] Mosek, Mosek modeling cookbook, https://www.mosek.com/.
[26] CPLEX, Ibm ilog, https://www.ibm.com/analytics/cplex-optimizer.
[27] Lobo MS, Vandenberghe L, Boyd S, Lebret H. Applications of second-order cone programming. Linear Algebr Appl 1998;284(1–3):193–228.
[28] Ben-Tal A, Nemirovski A. Lectures on modern convex optimization. Society for Industrial and Applied Mathematics; 2001.
[29] Makrodimopoulos A, Bhaskar A, Keane AJ. Second-order cone programming formulations for a class of problems in structural optimization. Struct Multidiscip Optim 2010;40(1–6):365–80.
[30] Rui K, Kanno Y. A mixed integer programming approach to designing periodic frame structures with negative Poisson's ratio. Optim Eng 2014;15(3):773–800.
[31] Kanno Y. Global optimization of trusses with constraints on number of different cross-sections: a mixed-integer second-order cone programming approach. Comput Optim Appl 2015;63(1):1–34.
[32] Kanno Y. Mixed-integer second-order cone programming for global optimization of compliance of frame structure with discrete design variables. Struct Multidiscip Optim 2016;54(2):1–16.
[33] Zowe J, Kocvara M, Bendsøe MP. Free material optimization via mathematical programming. Math Program 1997;79(1–3):445–66.
[34] Kocvara M, Zowe J. Free material optimization: An overview. Trends Ind Appl Math 2002;26(8):699–719.
[35] Stingl M, Kocvara M, Leugering G. A sequential convex semidefinite programming algorithm with an application to multiple-load free material optimization. Society for Industrial and Applied Mathematics; 2009, p. 130–55.
[36] Weldeyesus AG, Stolpe M. A primal-dual interior point method for large-scale free material optimization. Comput Optim Appl 2015;61(2):409–35.
[37] Podesta J, Mendez C, Toro S, Huespe A, Oliver J. Material design of elastic structures using Voronoi cells. Internat J Numer Methods Engrg 2018;115(3):269–92.
[38] Andreassen E, Clausen A, Schevenels M, Lazarov BS, Sigmund O. Efficient topology optimization in Matlab using 88 lines of code. Struct Multidiscip Optim 2011;43(1):1–16.
[39] Milton GW, Cherkaev AV. Which elasticity tensors are realizable? J Eng Mater Technol 1995;117(4):483–93.
[40] Allaire G. Shape optimization by the homogenization method, Vol. 146. Springer Science & Business Media; 2012.
[41] Hughes TJR. The finite element method: Linear static and dynamic finite element analysis. Prentice Hall; 2003.